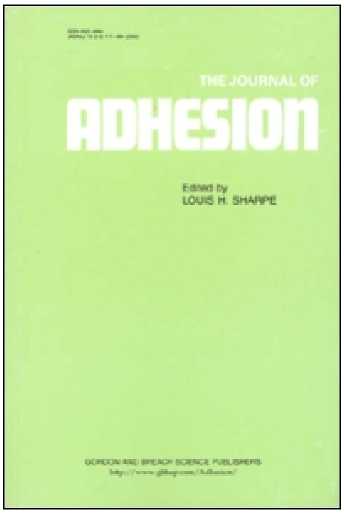

The Journal of Adhesion
Publication details, including instructions for authors and subscription information:
http://www.informaworld.com/smpp/title~content=t713453635

Local Dynamics of Bismaleimide Adhesives in an Aggressive Environment

Jovan Mijovic[a]; Nobuhiro Miura[a]; Hua Zhang[a]; Yuzhi Duan[a]
[a] Department of Chemical Engineering and Chemistry and The Herman F. Mark Polymer Research Institute, Polytechnic University, Brooklyn, New York, USA

To cite this Article Mijovic, Jovan , Miura, Nobuhiro , Zhang, Hua and Duan, Yuzhi(2001) 'Local Dynamics of Bismaleimide Adhesives in an Aggressive Environment', The Journal of Adhesion, 77: 4, 323 — 353
To link to this Article: DOI: 10.1080/00218460108030745
URL: http://dx.doi.org/10.1080/00218460108030745

The Journal of Adhesion, 77: 323–353, 2001

0021-8464/01 $12.00 +.00

LOCAL DYNAMICS OF BISMALEIMIDE ADHESIVES IN AN AGGRESSIVE ENVIRONMENT

Jovan Mijovic
Nobuhiro Miura
Hua Zhang
Yuzhi Duan
Department of Chemical Engineering and Chemistry and The Herman F. Mark Polymer Research Institute, Polytechnic University, Brooklyn, New York, USA

Molecular aspects of chemical and physical changes in bismaleimide (BMI) adhesive joints caused by absorbed moisture were investigated. The focus was on the early (pre-damage) stage that precedes the formation of voids and microcracks. Local dynamics were investigated by broad-band dielectric relaxation spectroscopy (DRS) and the changes in the chemical state of the matter were monitored by Fourier transform infrared spectroscopy (FTIR). Absorbed water interacts with the BMI network and gives rise to a fast relaxation process (termed γ^*), characterized by an increase in the dielectric relaxation strength, an Arrhenius temperature dependence of the average relaxation time, and an activation energy of 50 kJ/mol. The γ^* dynamics are slower than the relaxation of bulk liquid water because of the interactions between the absorbed water and various sites on the network (the ether oxygen, the hydroxyl group, the carbonyl group, and the tertiary amine nitrogen). One particularly significant finding is that the average relaxation time for the γ^* process above 20°C is of the order of nanoseconds or less and, hence, the detection and monitoring of this process hinges upon the ability to perform high precision DRS at frequencies above 1 MHz. This is an important consideration in the ongoing efforts aimed at the implementation of DRS as a non-destructive inspection (NDI) tool for adhesive joints. FTIR spectra reveal the presence of non hydrogen-bonded water and hydrogen-bonded water, the latter bonded to one and/or two sites on the BMI network. A good agreement was found between the calculated ratio of non hydrogen-bonded to total absorbed water from DRS and FTIR data.

Received 21 July 2001; in final form 12 October 2001.
This material is based on work supported by the AFOSR, Polymer Matrix Composites Program (Contract No. F49620-99-C-0057, Dr. Charles Y-C Lee, Program Director). One of the authors (JM) is most grateful to Professor Radomir Kovacevic for helpful comments.
Address correspondence to Jovan Mijovic, Department of Chemical Engineering, Polytechnic University, Six Metro Tech Center, Brooklyn, NY 11201, USA. E-mail: jmijovic@poly.edu

Keywords: Adhesive; Environmental exposure; Dielectric relaxation spectroscopy; Local dynamics

INTRODUCTION

The under-utilization of adhesive joints, particularly in aerospace structures, is a widely recognized phenomenon that is largely ascribed to an insufficient fundamental understanding of the effect of the service environment on these joints. The consensus of opinion is that the chemical and physical changes in the adhesive on a *molecular level* during the early (pre-damage) stage of environmental exposure (prior to the formation of voids and microcracks that lead to the degradation of joints) hold the key to the understanding of initiation, propagation and failure [1]. The vast majority of the reported studies, e.g. [2–16], however, have been concerned with the effect of moisture on *macroscopic* (bulk) properties and/or the detection of delamination and loss of adhesion that occur when water eventually diffuses through the adhesive and reaches the adhesive/adherend interface/interphase.

There are numerous fundamental questions about the *molecular-level* events in glassy adhesives in the pre-damage stage that remain unanswered. In what form (single molecules, dimers, trimers, hydrogen-bonding complexes) does the absorbed water reside in the adhesive? How does water interact with the host matrix and what effect does it have on the local network dynamics? What are the effects on dynamics of the temperature, pressure and relative humidity of the environment? The knowledge gained from such studies is expected to contribute further towards the development of a methodology that can predict the course of subsequent degradation and anticipate failure.

The paucity of information about the effect of absorbed moisture on the local dynamics in glassy adhesives is caused to a large measure by the short time scale (as fast as few picoseconds and, hence, not easily measured) of these processes. Of the few experimental techniques operable at high frequency (where fast processes are observed) and adaptable to the adhesive joint configuration, broad-band dielectric relaxation spectroscopy (DRS) is rapidly becoming a dominant tool [17, 18], and it was utilized in this study. The great attraction of DRS derives from an unparalleled frequency range available (up to 16 decades) that enables one to conduct fundamental studies of molecular dynamics of condensed matter in various phases and at different temperatures: from amorphous liquids to liquid crystals to an amorphous or crystalline glass; from high temperature, where the dipole relaxation times are on the order of picoseconds, through the vitrification process, where relaxation times in the glassy state reach tens to hundreds of seconds. Of course, the interpretation of molecular dynamics obtained from DRS can be greatly aided with the use of a complementary technique capable of providing specific information about the *chemical state* of the matter. Among those techniques, Fourier Transform Infrared Spectroscopy (FTIR) represents the most attractive choice because of: (1) the unmatched wealth of information about the chemical state of the matter contained in the infrared spectrum, (2) the adaptability of near-IR (NIR) to remote (fiber-optic) *in-situ* real-time applications, and (3) the possibility of using NIR for non-destructive inspection (NDI). The combined use of DRS and FTIR spectroscopy is, therefore, designed to afford a simultaneous examination of *physical* (DRS) and *chemical* (FTIR) changes at a molecular level in adhesive joints exposed to an aggressive environment.

Our initial efforts along those lines are described in a recent publication that deals with the effect of absorbed moisture on the *chemical and physical* changes in epoxy-amine adhesive joints [18]. Here, we focus attention on the effect of moisture on the local dynamics of a two-component bismaleimide (BMI) formulation.

THEORETICAL BACKGROUND

We describe the theoretical basis of DRS briefly, and for further details we refer the interested reader to one of the several excellent reviews in the literature [19, 20]. In an isotropic amorphous system, with negligible internal field factors, the complex dielectric permittivity, ε^*, is related to the dipole moment correlation function by [21]:

$$\frac{\varepsilon^*(\omega) - \varepsilon_\infty}{\varepsilon_0 - \varepsilon_\infty} = 1 - i\omega \int_0^\infty [\exp(-i\omega t)]\Phi(t)dt \tag{1}$$

where ε_0 is the limiting low-frequency value of the dielectric permittivity, ε_∞ is the limiting high-frequency dielectric permittivity, ω is angular frequency, and $\Phi(t)$ is the relaxation kernel that can be obtained, theoretically, from the dipole moment time-correlation function (TCF) [21]. The reorientational motion of dipoles gives rise to a relaxation process in the frequency domain, and the physical interpretation of this behavior is understood in terms of the dipole moment TCF. Traditionally, it bas been customary to present the results of DRS by analytical fits of ε^* (ε' and/or ε'') in the frequency domain using various empirical functional forms. For example, ε^* may be modeled by a number of empirical functions in the frequency domain; a particularly popular and robust form is the Havriliak-Negami (HN) [22] function, given as:

$$\varepsilon^*(\omega) = \varepsilon_\infty + \frac{\varepsilon_0 - \varepsilon_\infty}{[1 + (i\omega\tau_{HN})^a]^b} + i\frac{\sigma}{\omega\varepsilon_v} \tag{2}$$

where a and b are the dispersion shape parameters, σ is the conductivity, ε_v is the vacuum permittivity, and the other parameters are defined in Eq. (1). The HN equation is a generalization of the Cole-Cole (CC) equation, to which it reduces for $b = 1$, and a generalization of the Cole-Davidson (CD) equation, to which it reduces for $a = 1$. HN and CC functional forms were employed in this study to describe local dynamics in the frequency domain. Alternatively, the dipole moment correlation function can be quantified *via* a stretched exponential function of the Kohlrausch-Williams-Watts [23] (KWW) type:

$$\Phi(t) = Ce^{-(t/\tau)^\beta} \tag{3}$$

where C is a constant, τ is the relaxation time, and β is the stretching exponent ranging from 0 to 1 ($\beta = 1$ for the single exponential decay function). The average relaxation time is defined as $\tau = 1/2\pi f_{\max}$, where $f_{\max}$ is the frequency of maximum loss. Typically, the temperature dependence of τ is of the Vogel-Fulcher-Tammann (VFT) form for the segmental relaxation (the α process) and of the Arrhenius form for the localized sub-Tg processes (*e.g.*, the β process).

EXPERIMENTAL MATERIALS

A two-component bismaleimide (BMI) formulation (Matrimid 5292, courtesy of Ciba-Geigy Corporation), consisting of 4,4′ bismaleimidodiphenyl methane (component A) and 0,0′ diallyl bisphenol A (component B), was investigated in this study. Chemical structures of components A and B are shown in Figure 1. Equimolar amounts of the two components were mixed at 120−125°C and stirred continuously until a clear, homogeneous mixture was obtained. The cure schedule consisted of heating the sample from 20 to 240°C at 5°C/min and maintaining it at 240°C for 30 min. Samples were cured between aluminum adherends, and the calorimetric (DSC) glass transition temperature (Tg) was over 220°C. The adherend surface was cleaned with acetone prior to the application of the resin. The bondline thickness was 50 μm. The cured samples were reproducible (DSC and FTIR controls were run) and were subjected to the identical thermal history (by heating above the Tg and then cooling) prior to the exposure to the environment to factor out the effect of structural

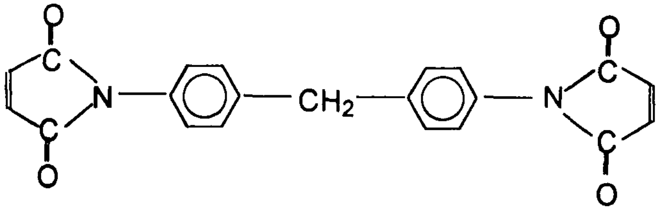

Component A

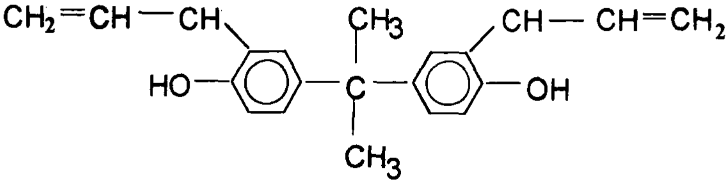

Component B

FIGURE 1 Chemical composition of the BMI formulation.

relaxation *between* different samples. Two controlled aggressive environments were employed: (1) 60°C/98 %RH, and (2) 80°C/98 %RH. Relative humidity (RH) was maintained with a saturated $NaHSO_4$ solution. Samples were removed from the environment at selected time intervals and tested.

TECHNIQUES

The principal experimental technique we used was broad-band dielectric relaxation spectroscopy (DRS). A brief description of our experimental facility for dielectric measurements follows. More details are given elsewhere [24], and several excellent reviews of experimental methodology for dielectric measurements were recently published [25, 26]. In this study we have used Novocontrol's α Analyzer (3 µHz–10 MHz) and a Hewlett-Packard 4291 B RF Impedance Analyzer (1 MHz–1.8 GHz). Both instruments are interfaced to computers *via* IEEE 488.2 and are connected to a heating/cooling unit (modified Novocontrol's Novocool System) equipped with a custom-made motor driven arm that can selectively insert into the Novocool cryostat chamber either the low-frequency or the high-frequency sample cell. This configuration has the advantage of providing high-precision temperature control over the entire frequency range (3 μHz– 1.8 GHz). A variety of sample cells were employed, including parallel plates, high precision extension airlines, cells for the simultaneous dielectric/remote fiber optic FTIR tests, etc. Supporting evidence was obtained from FTIR spectroscopy, using Nicolet Instrument's Magna 750 Spectrometer [27], and differential scanning calorimetry (DSC), using Perkin-Elmer model 7 DSC at a heating rate of 10°C/min.

RESULTS AND DISCUSSION

We begin by presenting the DRS results for the uncured BMI (the initial mixture of components A and B). This system is miscible and has a calorimetric (DSC) Tg of − 20°C prior to the onset of curing reactions. Dielectric permittivity and dielectric loss in the frequency domain (measured over 11 decades of frequency) with temperature as a parameter are shown in Figure 2. Because permittivity and loss are related by the Kramers-Kronig transforms, the remaining figures in the text contain only the loss data. The solid lines in Figure 2 are fits to the HN functional form (Eq. (2)) with the low frequency contribution subtracted. The data depict the segmental α process above the calorimetric Tg of the mixture. The temperature dependence of the average relaxation time, defined as $\tau = 1/2\pi f_{\mathrm{max}}$, is of the Vogel-Fulcher-Tammann (VFT) form. We reiterate that the uncured system is shown only as a reference, and all subsequent results pertain to the cured networks with a calorimetric Tg above 220°C. Dielectric loss in the frequency domain for a cured dry network, with temperature as a parameter, is shown in Figure 3. In this temperature range, the network is well below its Tg, and we measure the loss due to the local relaxation. We observe a prominent β process that is characterized by: (1) an increase in the dielectric relaxation strength ($\Delta\varepsilon$) with increasing temperature and (2) an Arrhenius temperature dependence of the average relaxation time, τ. Interestingly, the loss spectra are narrower than usually observed for the so-called Johari-Goldstein β process [28] in molecular or polymeric glass formers. We also note a low but measurable loss at frequencies above 10 kHz, suggesting the presence of a relaxation that is faster (more local) than β. The loss intensity of this relaxation increases with increasing temperature, and we term this process γ. Owing to their local nature, the β and γ processes are

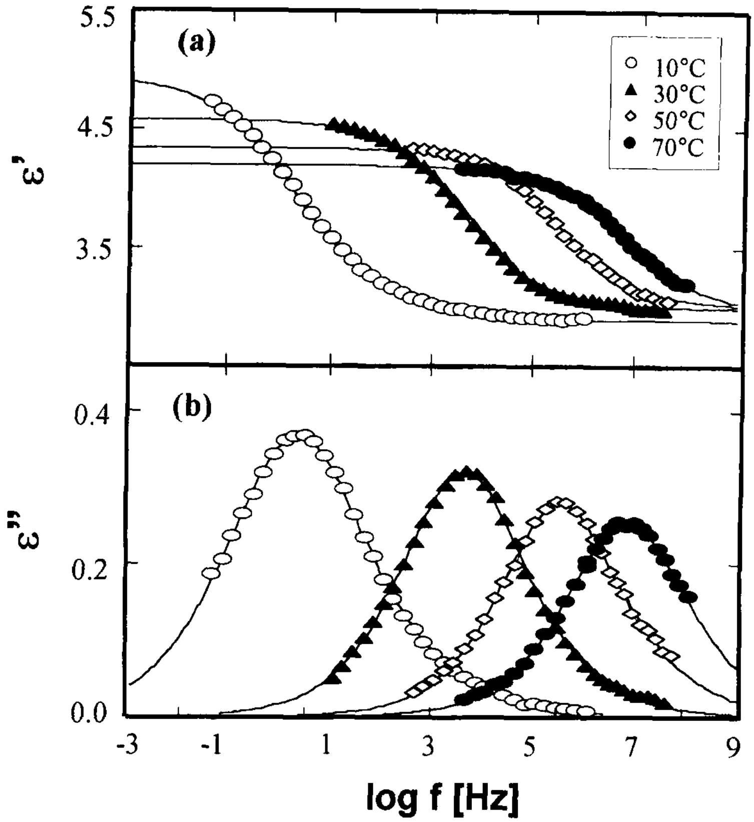

FIGURE 2 (a) Dielectric permittivity and (b) loss in the frequency domain for uncured BMI with temperature as a parameter. Solid lines are fits to the Havriliak-Negami equation.

precisely what we are interested in; we shall not be concerned here with the α dynamics because our networks are well into the glassy state under the conditions of this study. The molecular origin of the β process is in the rotation around phenyl-oxygen bonds. The γ process, however, is strongly affected by the absorbed moisture, and we shall return to its origin later.

Once the dielectric response of the cured dry network was established, we proceeded with a systematic study of the effect of absorbed moisture on the local dynamics. We preface the presentation and discussion of these results with two comments. First, we stress that we shall not principally be concerned here with the kinetics of moisture absorption, *e.g.*, [29–31]. And second, we acknowledge a number of

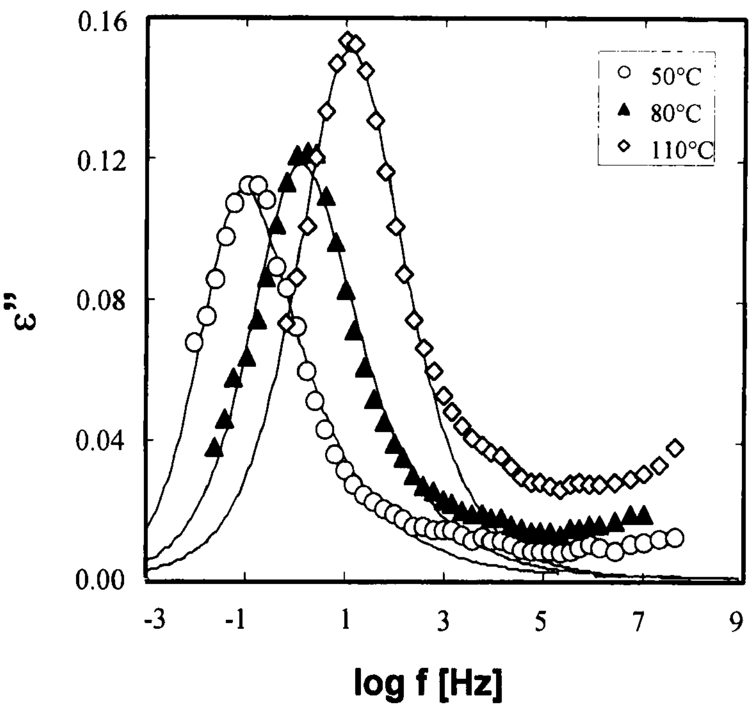

FIGURE 3 Dielectric loss in the frequency domain for cured BMI with temperature as a parameter. Solid lines are fits to the Havriliak-Negami equation.

efforts to monitor moisture absorption in polymer networks quantitatively by tracking dielectric permittivity at a constant frequency [32–36], but hasten to add that the dielectric response of a changing structure is a function of both exposure time *and* frequency. Therefore, when one is interested in dynamics, as we are here, the correct way to track it is by recording the relaxation spectra at selected time intervals over a wide frequency range. Because of the local nature of the sub-Tg relaxations, it was anticipated that the dynamics of such processes would be particularly sensitive to the presence of absorbed moisture from the very beginning of the environmental exposure.

Let us now examine the loss spectra *measured* at select temperatures following exposure to the 60°C environment for various times. Figure 4 shows dielectric loss in the frequency domain measured at 50°C for samples exposed to the environment for 3 and 5 days. A spectrum of the dry sample is also included as a reference. There is a remarkable change in the relaxation spectrum as a result of the moisture uptake. We observe the emergence of a pronounced

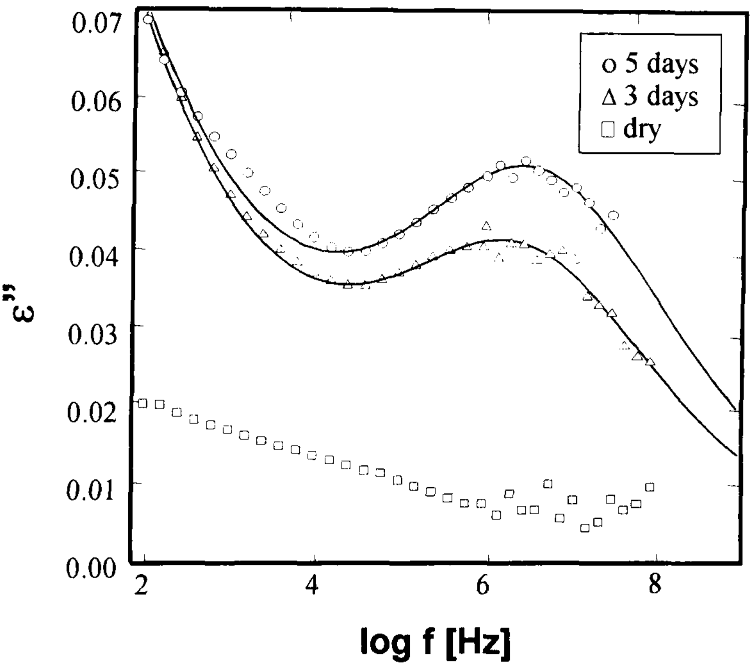

FIGURE 4 Dielectric loss in the frequency domain measured at 50°C for 0-, 3- and 5-day exposure to 60°C/98% RH.

relaxation with an average relaxation time of about 8 ns, corresponding to the frequency at the loss maximum of *ca.* 20 MHz. The intensity of this process, which we term γ^*, increases with exposure time. It is clear that the γ^* process *is not* a modified (by absorbed moisture) β process; note that the β process in the dry sample, at the same temperature of 50°C (Figure 3), is located at about 0.1 Hz, a full seven decades lower. Apparently, the γ^* process originates in the interactions of the absorbed moisture with the γ^* process observed in the dry sample. With decreasing measuring temperature, the γ^* process moves to lower frequency, as exemplified in Figure 5a–c measured at −20, −60, and −100°C, respectively. Analogous observations were made in the samples exposed to the 80°C environment for various times between 30 minutes and 2 days, as seen in Figure 6a–c, measured at 20, −20, and −60°C, respectively. The gradual emergence of a loss peak is noted in each figure. Interestingly, the frequency of maximum loss increases initially (the average relaxation time gets shorter) and then levels off, while loss intensity increases continuously with exposure time. When samples exposed to 60 and 80°C

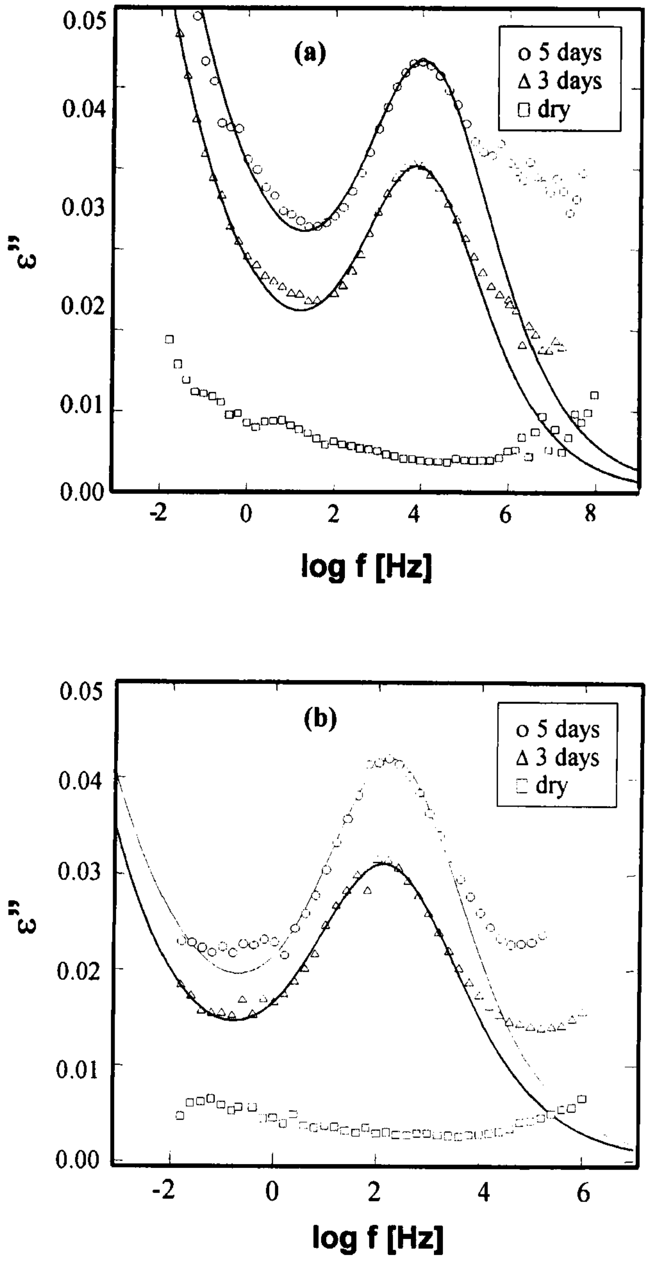

FIGURE 5 Dielectric loss in the frequency domain for cured BMI exposed to 60°C/98% RH with exposure time as a parameter, measured at (a) −20°C, (b) −60°C, and (c) −100°C.

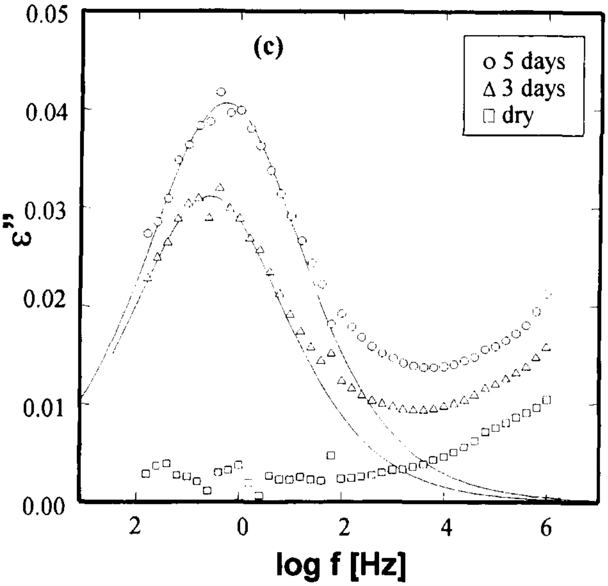

FIGURE 5 (*continued*)

environments for the same duration are compared at the same measuring temperature, we note an increase in intensity for the latter batch. All fits in Figures 5 and 6 are to the CC functional form. We have also generated KWW fits but have not observed a systematic variation in the KWW β parameter for those samples. The calculated average value of β_{KWW} of about 0.3 is below that for the segmental α process, but slightly above a typical value for the localized β process in molecular and polymeric glass-formers.

An alternative way of displaying the effect of absorbed moisture on the local dynamics is to plot the loss spectrum at a fixed exposure time and with temperature as a parameter. An example is shown in Figure 7a–b, for the 60°C environment and exposure times of 3 (7a), and 5 (7b) days, respectively. Note the systematic shift of the γ^* process to lower frequency with decreasing temperature.

A composite plot of the frequency of maximum loss for different relaxation processes and environments is shown as a function of reciprocal temperature in Figure 8. Both the β process (in dry BMI) and the γ^* process are Arrhenius, with an activation energy of about 80 kJ/mol and 50 kJ/mol, respectively. Data in Figure 8 for the γ^* process correspond to the exposure times where further moisture absorption does not affect the average relaxation time. We observe that

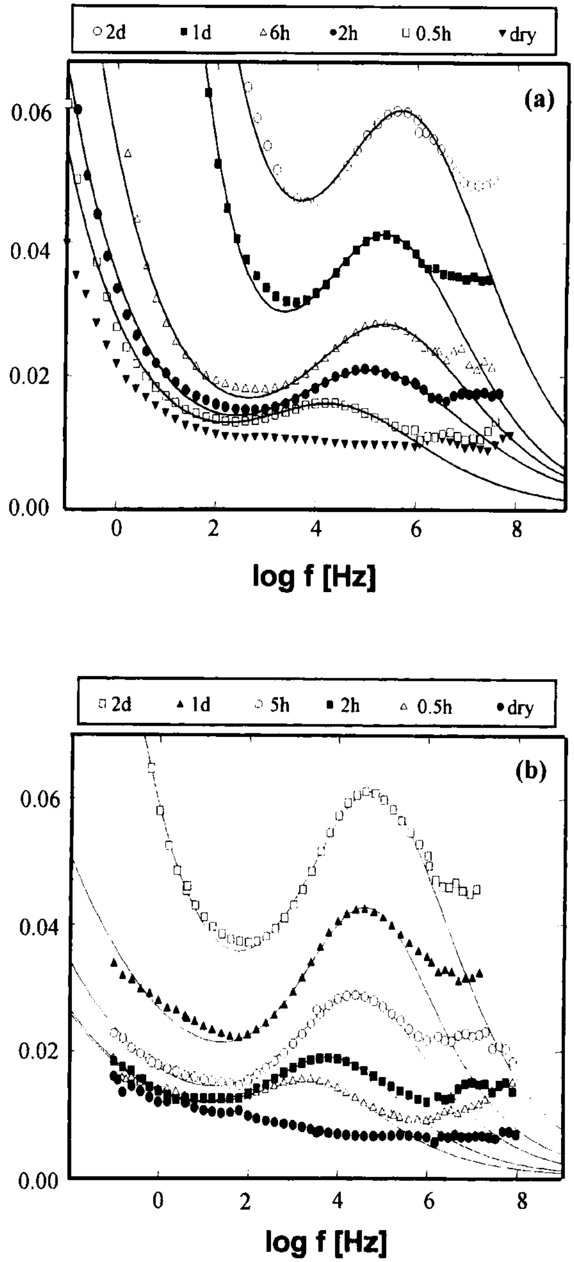

FIGURE 6 Dielectric loss in the frequency domain for cured BMI exposure to 80°C/98% RH, with exposure time as a parameter, measured at (a) 20°C, (b) −20°C, and (c) −60°C.

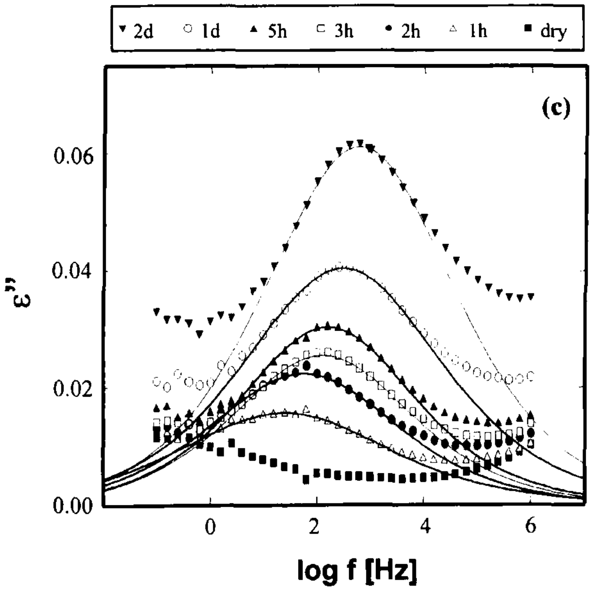

FIGURE 6 *(continued)*

the data for the 60 and 80°C environments fall on the same line and yield the same activation energy.

Next, we examined the dielectric relaxation strength, $\Delta\varepsilon$, of the γ^* process. $\Delta\varepsilon$ is an important material characteristic because it depends on the chemical structure and molecular architecture. Relaxation strength is defined as $\Delta\varepsilon = \varepsilon_0' - \varepsilon_\infty'$, where ε_0' and ε_∞' represent the limiting low- and high-frequency dielectric permittivity, respectively, and is proportional to the concentration of dipoles and the mean-squared dipole moment per molecule. The possibility of analyzing dielectric relaxation strength in terms of component contributions and, for each component, in terms of molecular dipole moments, is of particular interest to us. If the concentration of each dipolar group could be obtained from the FTIR measurements, the change in the chemical/molecular architecture during moisture absorption could be monitored *in-situ* by DRS. With this information, the classic Onsager (or appropriately modified) model could be used as a starting point in the attempt to develop a relationship between chemical and physical changes in moisture-absorbing networks. The Onsager model [37] is written as:

$$\frac{(\varepsilon_0 - \varepsilon_\infty)(2\varepsilon_0 + \varepsilon_\infty)}{\varepsilon_0(\varepsilon_\infty + 2)^2} = \frac{\sum N_i \langle \mu_i^2 \rangle}{9kT\varepsilon_v} \tag{4}$$

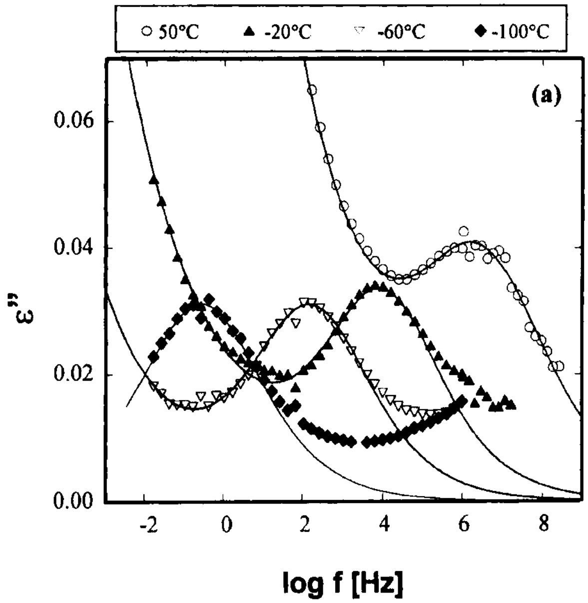

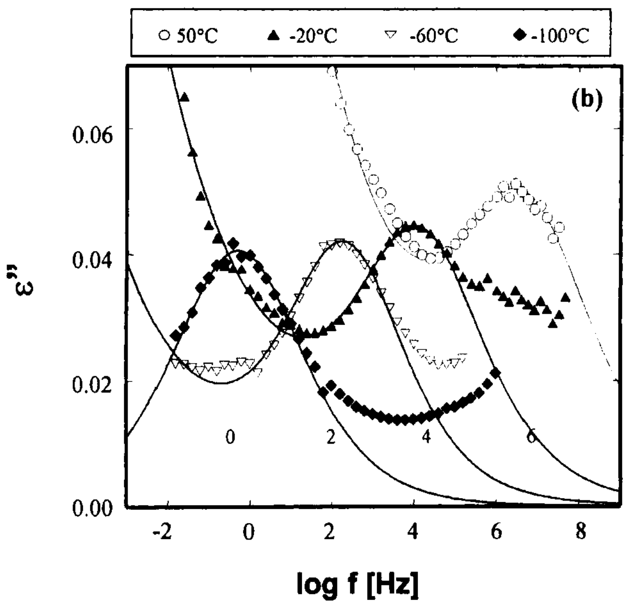

FIGURE 7 Dielectric loss in the frequency domain for cured BMI after (a) 3 days, and (b) 5 days of exposure at 80°C/98% RH, with temperature as a parameter.

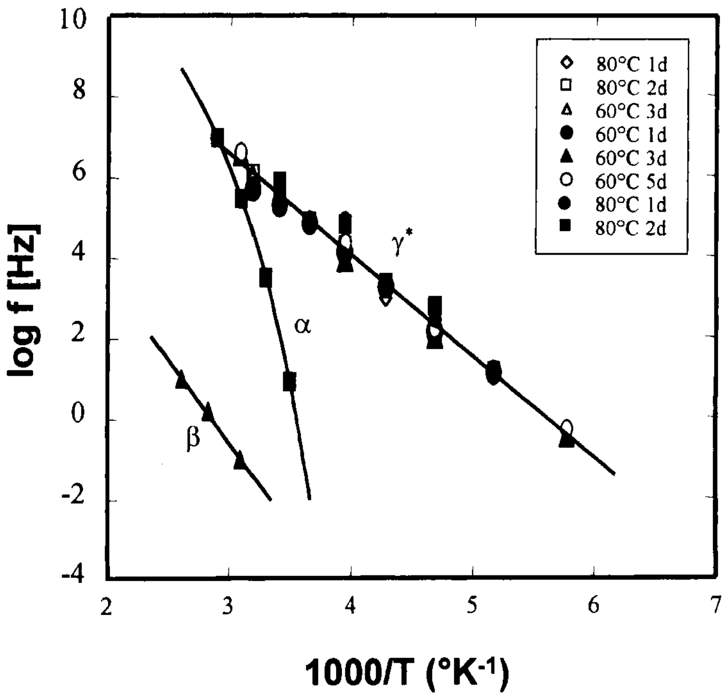

FIGURE 8 Log frequency at maximum loss as a function of reciprocal temperature for different exposure times in dry and moist BMI.

where ε'_0 and ε'_∞ are the limiting low- and high-frequency permittivities, N_i is the dipole concentration of species i (dipoles/cm^3), $\langle \mu_i^2 \rangle$ is the ensemble average dipole moment squared of molecule i, T is the temperature, and ε_v is the vacuum permittivity. The ability to identify and measure precisely the concentration of a particular dipole group (or an interactive hydrogen-bonded complex) raises interesting possibilities with respect to the correlation between vibrational and dielectric spectroscopy. In Figure 9, we show a composite plot of dielectric relaxation strength as a function of exposure time at 60 and 80°C, with measuring temperature as a parameter. The data reveal that: (1) $\Delta\varepsilon$ increases with exposure time in both aggressive environments, and (2) $\Delta\varepsilon$ increases faster at a higher exposure temperature. It is clear that moisture absorption is accompanied by an increase in the concentration of dipoles, suggesting a correlation between $\Delta\varepsilon$ and molecular composition (an investigation is currently underway in our laboratory).

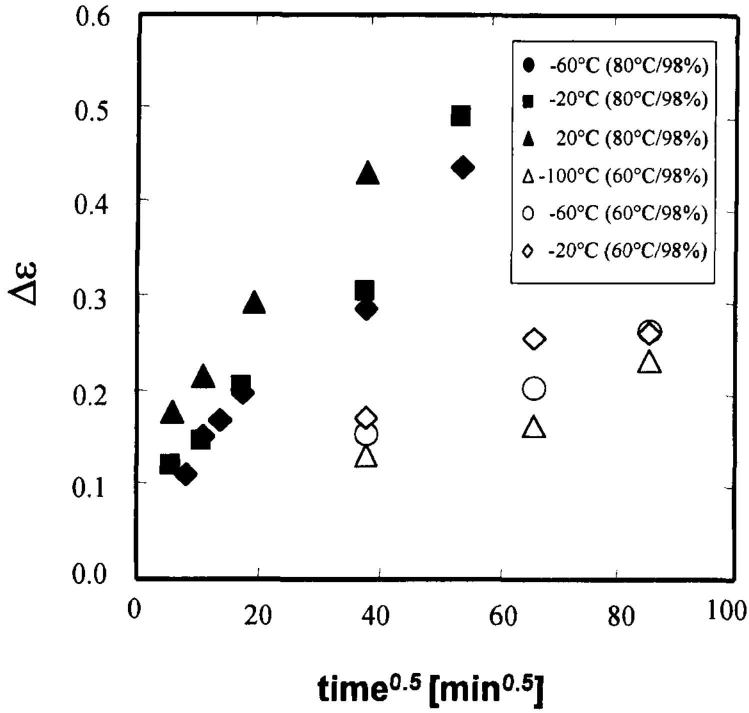

FIGURE 9 Dielectric relaxation strength of cured BMI after exposure to 60 and 80°C environments as a function of exposure time.

An important question is what can be learned from the DRS data about the molecular origin of the sub-Tg relaxations and the γ^* process in particular. Although the precise nature of the interactions between the network and the absorbed moisture would be elucidated only in conjunction with the FTIR data, it is immediately clear that the γ^* process is strongly affected by water. What is not clear from DRS data are the following issues: 1) in what form does (*e.g.*, isolated single molecules, dimers, trimers) water reside within the adhesive, 2) at which network sites does water form hydrogen bonds, and 3) how many hydrogen bonds are formed by water molecules? An examination of all these questions is offered later in the text. We acknowledge the excellent work of Musto *et al.* [38, 39], who reported that water molecules in epoxy-amine networks participate in hydrogen bonding at one or two sites in the network.

Notwithstanding the form in which water resides in the adhesive, a comparison with the dynamics of liquid water is warranted. For example, at 50°C liquid water has a dielectric loss peak at about 25 GHz (corresponding to an average relaxation time of about 9 picoseconds) [40], while the relaxation time of the γ^* process at the same temperature is longer by about three decades on the frequency scale. Whether the reason for this is physical (*e.g.*, steric hindrance due to neighboring moieties, such as benzene rings) and/or chemical (hydrogen bonding interactions with specific network sites) is not apparent from DRS. The findings reported by Jelinski *et al.* [41, 42] in their study of epoxy networks by solid state NMR spectroscopy are similar. These authors also argue that the "free" water (defined as isotropically mobile with the same relaxation time as liquid water) is not present in the network. The γ^* process in BMIs, with an average relaxation time of 160 ps at 20°C, is slower than the γ process in moist epoxy-amine networks, but faster than the β process in these networks [18].

Formation of hydrogen bonds throughout the network is expected to affect the dynamics. Identification of the network sites that could form hydrogen bonds with absorbed moisture requires knowledge of the molecular architecture, which, in turn, requires an understanding of the reaction mechanism that leads to network formation. While only a few such studies have been reported, the complexity of BMI cure is widely recognized [43–49]. Suffice it to say that a number of polymerization and cross-linking routes have been claimed, including homopolymerization of BMI *via* the reaction of the maleimide C=C double bond that results in the formation of four-member rings, homopolymerization of BMI *via* the reaction of the maleimide C=C that involves three BMI molecules, reaction between the maleimide double bonds and allyl groups, homopolymerization of allyl double bonds, etherification (dehydration) involving hydroxyl groups of the allyl component, etc. Based upon the earlier investigations of the effect of cure conditions on the reaction kinetics, mechanism, and structure of BMI networks [48], we can say that the thermal history used in this study will give rise to a network schematically shown (characteristic fragment) in Figure 10. An examination of this figure reveals several possible sites (hydroxyl group, ether oxygen, carbonyl group, tertiary amine nitrogen) that could participate in hydrogen bonding with absorbed moisture (shown in bold, Figure 10). After examining this issue further, we raise two important questions. First, is there an order of preference with respect to the network site for hydrogen bond formation? And second, is it possible to determine the number of network sites to which each water molecule bonds? It was anticipated that further insight into these queries would be obtained from the FTIR study; hence, we turn attention to the results of the near-IR (NIR) and mid-IR (MIR) analyses of our networks. We acknowledge the use of

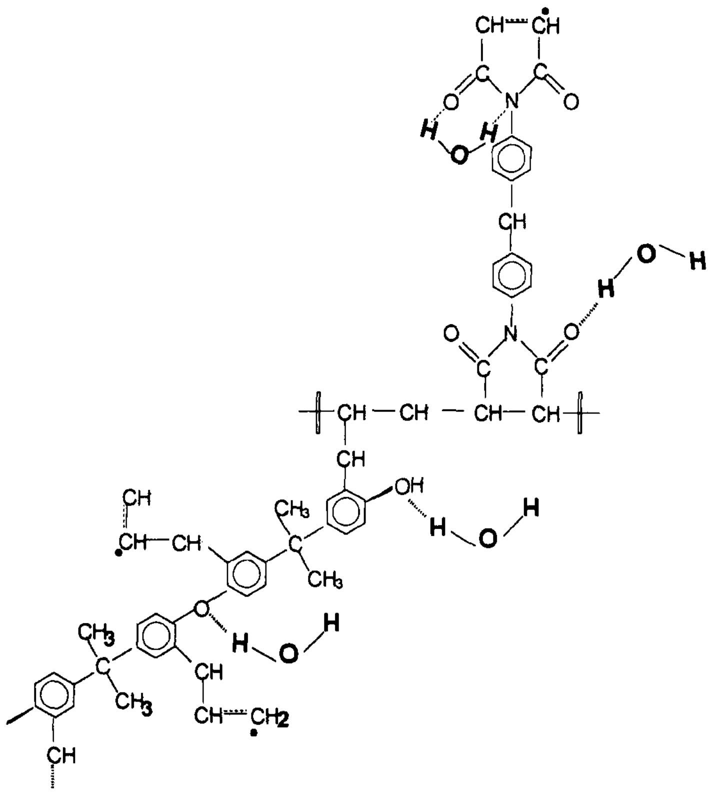

FIGURE 10 Chemical structure of a fragment of the cured BMI network. Note: Different network sites that could participate in hydrogen bonding with absorbed water are shown in bold.

conventional FTIR spectroscopy to detect moisture in polymers [50–53], but are not aware of any study of adhesive joints by a combined NIR, MIR and DRS approach.

NIR and MIR spectra of the individual components (A and B) of our BMI formulation have been documented elsewhere [48] and will not be described here. A NIR spectrum of the cured dry network (top line in Figure 11a) contains all major peaks of relevance, including hydroxyl absorption around 7000 cm^{-1}, allyl and maleimide double bond absorption at 6112 cm^{-1} and a doublet due to the –CH stretching (4627, 4676 cm^{-1}). The broad absorption between *ca.* 5750 and 5900 cm^{-1} has been shown [48] to contain three peaks characteristic of the homopolymerized maleimide (component A). A series of NIR spectra of

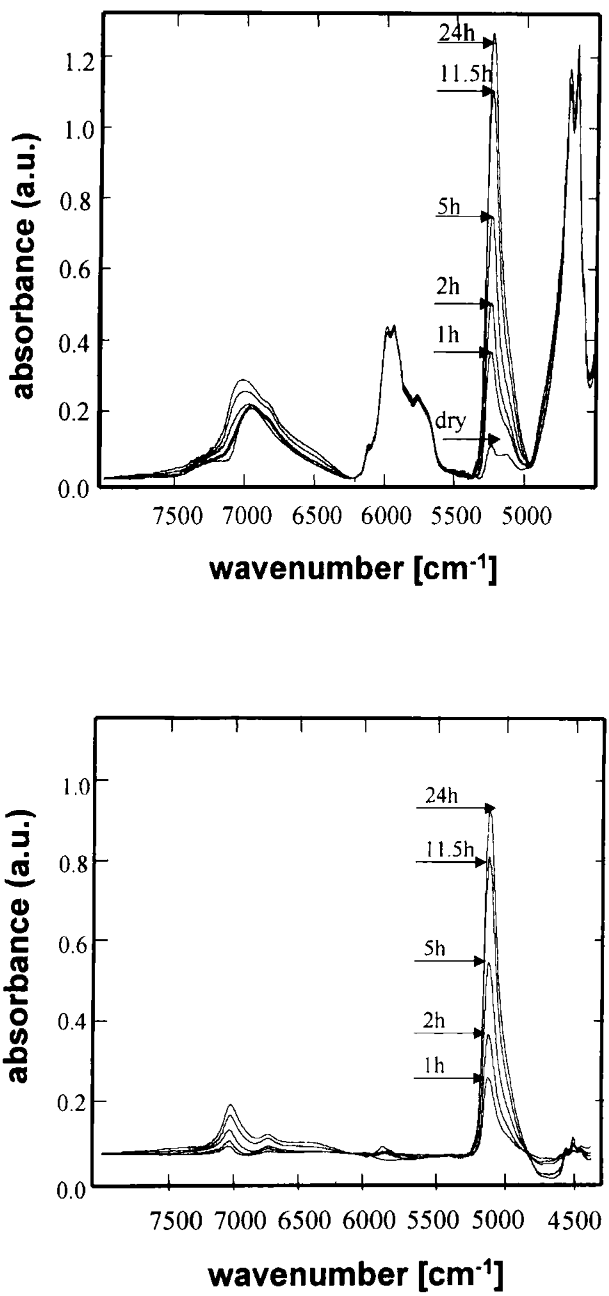

FIGURE 11 (a) NIR spectra of BMI at different exposure times: dry, 2 h, 1 day, 4 days, and 23 days; (b) difference spectra.

moist samples taken at select time intervals during exposure to the 80°C environment are also shown in Figure 11a. Difference spectra obtained by subtraction, using the 5500–6200 cm^{-1} range as the internal standard, are shown in Figure 11b. Water uptake causes pronounced changes in the 4950–5400 cm^{-1} and 6200–7500 cm^{-1} range; we examine the former first. There is a progressive increase in the intensity of the absorption band centered at 5225 cm^{-1} that has been associated with the combination band due to bending (deformation) (1600–1650 cm^{-1}) and asymmetric stretching (3100–3800 cm^{-1}) of (the absorbed) water. A careful inspection of the data also reveals a consistent increase in the absorption intensity at the lower wavenumber (lower frequency) side of the 5225 cm^{-1} peak, suggesting a gradual development of a parallel absorption mechanism. This is an interesting finding. Deconvolution of the broad absorption was accomplished and two absorption peaks were clearly detected, as exemplified in Figure 12. Both peaks were Gaussian; initially, the first

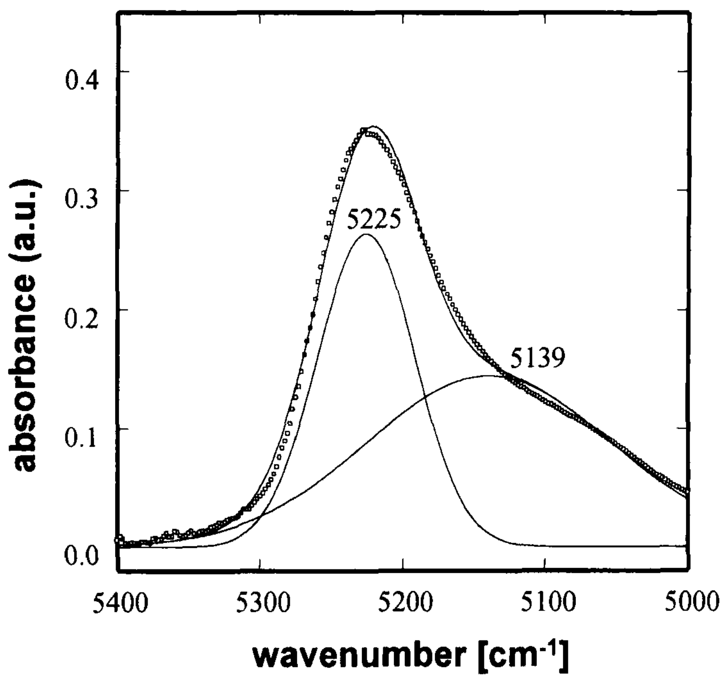

FIGURE 12 Deconvoluted difference spectra in the 5000–5400 cm^{-1} range after a 1-day exposure to 60°C /98% RH.

was centered at 5225 cm^{-1} and the second at 5116 cm^{-1}. During exposure, the second peak exhibited a slight shift to higher wavenumber (frequency). Interestingly, the area under each peak is a linear function of water content. Unfortunately, identification of each peak with specific interactions (although of considerable interest) is difficult because the NIR absorption in this range is associated with the overtones of a combination of bending and stretching vibrations that are affected oppositely by hydrogen bonding; therefore, no further attempts were made along those lines.

Additional information was obtained from the consideration of the characteristic hydroxyl absorption in the 6200–7500 cm^{-1} region. Deconvolution of the spectra [54] reveals the presence of three absorption bands (following a 2-hour exposure to 80°C) centered at 7088, 6804 and 6445 cm^{-1}, as seen in Figure 13. Similar observations were reported in other systems, including the liquid mixtures of water

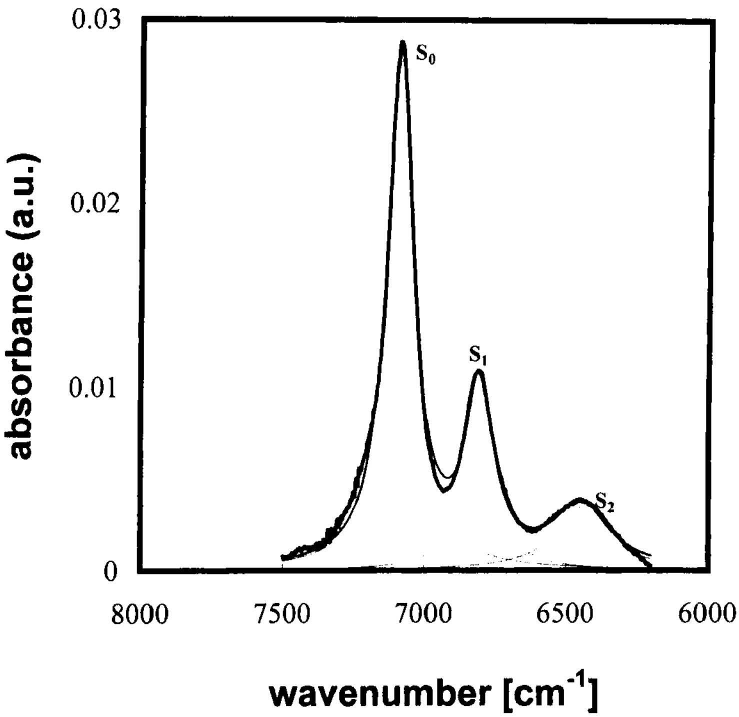

FIGURE 13 Deconvoluted NIR spectrum of cured BMI after exposure to 80°C for 5 h.

with non-polar and polar solvents, and cross-linked thermoset networks [55, 39]. An explanation was offered by postulating the existence of three spectroscopically distinguishable forms of hydrogen bonding, termed S_0, S_1 and S_2, where subscripts zero, one and two denote the number of hydrogen atoms of the water molecule that participate in hydrogen bonding. Based on the changes in the breadth and the full width-at-half-height (fwhh) of the peaks at 7088, 6804 and 6445 cm^{-1}, an argument can be postulated to associate these absorption bands with S_0, S_1 and S_2, respectively. Although the fwhh of each peak did not change with water uptake, the fwhh of the 6445 cm^{-1} band was about two-three times greater than the other two. This further supports the assignment of the 6445 cm^{-1} band to strong hydrogen bonding interactions likely to be encountered in S_2 complexes.

An important consideration is the proportion of non-hydrogen-bonded to hydrogen-bonded water absorbed in the network. We have monitored the increase in the peak area of the corresponding absorption bands during moisture uptake and have calculated the S_0/S_t ratio, where $S_t = S_0 + S_1 + S_2$. The absorbance area, A, is related to the concentration of the absorbing species, C, by $A = aC$, where a is the absorption coefficient. We extended Choppin's finding [55] that the absorption coefficient for S_0, S_1 and S_2 in water-solvent systems did not vary with the type of solvent in our BMI network, and we utilized his values for a_1, a_2 and a_3. The following equation was then used to calculate the relative concentration of each species ($i = 0$, 1 or 2):

$$\frac{C_{Si}}{C_{tot}} = \frac{A_i/a_{S_1}}{A_{7088}/a_{S_0} + A_{6804}/a_{S_1} + A_{6445}/a_{S_2}} \tag{5}$$

The relative ratios of various forms of absorbed water are plotted as a function of water content in Figure 14. It is very interesting to note that about 70% of the absorbed water is in the S_0 form and that the ratio of any absorbed species (S_0, S_1 or S_2) to the total absorbed water changes very little with moisture uptake.

The DRS data were also utilized for an analogous calculation. We assume that the local dynamics in our networks are characterized by two processes: (1) the γ^* process, representing the dynamics associated with the S_1 and S_2 forms; and (2) the δ process, representing the dynamics of the non-hydrogen-bonded water (S_0) that relaxes at frequencies above 10^{10} Hz. We then calculate the S_0/S_t ratio from the DRS data by manipulating the left-hand side (LHS) of the Onsager equation (Eq. (4)) into the following form:

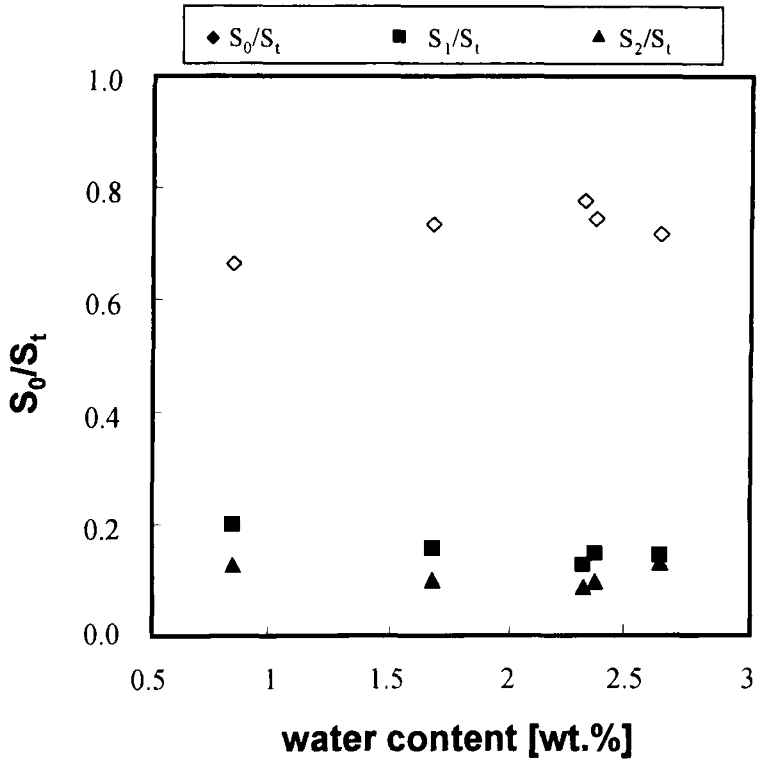

FIGURE 14 Ratio of various non-hydrogen-bonded (S_0) and hydrogen-bonded (S_1, S_2) species to total (S_t) absorbed water as a function of water content, calculated from the NIR data.

$$\frac{\left[\frac{(\varepsilon'_{1\,\mathrm{MHz}}-\varepsilon_\infty)(2\varepsilon'_{1\,\mathrm{MHz}}+\varepsilon_\infty)}{\varepsilon'_{1\,\mathrm{MHz}}(\varepsilon_\infty+2)^2}\right](m)-\left[\frac{(\varepsilon'_{1\,\mathrm{MHz}}-\varepsilon_\infty)(2\varepsilon'_{1\,\mathrm{MHz}}+\varepsilon_\infty)}{\varepsilon'_{1\,\mathrm{MHz}}(\varepsilon_\infty+2)^2}\right](dry)}{\left[\frac{(\varepsilon'_{0.1\,\mathrm{Hz}}-\varepsilon_\infty)(2\varepsilon'_{0.1\,\mathrm{Hz}}+\varepsilon_\infty)}{\varepsilon'_{0.1\,\mathrm{Hz}}(\varepsilon_\infty+2)^2}\right](m)-\left[\frac{(\varepsilon'_{0.1\,\mathrm{Hz}}-\varepsilon_\infty)(2\varepsilon'_{0.1\,\mathrm{Hz}}+\varepsilon_\infty)}{\varepsilon'_{0.1\,\mathrm{Hz}}(\varepsilon_\infty+2)^2}\right](dry)}=\frac{S_0}{S_t} \quad (6)$$

In Eq. (6), the values ε' at 0.1 Hz and 1 MHz have the same physical significance as described above and those two frequencies were selected for the following reason. The value of ε' at 0.1 Hz represents the limiting low-frequency permittivity that encompasses both the γ^* and δ processes (*i.e.*, 0.1 Hz $\ll \omega_{\mathrm{max}\gamma^*}$; Figure 5). The value of ε' at 1 MHz was taken to represent the limiting low-frequency permittivity for the δ process (*i.e.*, 1 MHz $\ll \omega_{\mathrm{max}\delta}$). Thus, by tracking the changes in ε' at 0.1 and 1 MHz during moisture uptake, one gets information about the increase in the total ($S_t = S_0 + S_1 + S_2$; denominator of Eq. (6)) and non-hydrogen-bonded (S_0; numerator of Eq. (6)) water, respectively. The value of ε_∞, the limiting high-frequency permittivity for our network was set equal to 2.5. This value was estimated, due to our inability to obtain it directly from experiment; (the experimental frequencies required are beyond present instrumental means, and the Maxwell relation between n^2 (where n is the sodium D-line refractive index) $= \varepsilon_\infty$, contains uncertainties arising from very-high-frequency secondary and phonon absorptions. The S_0/S_t ratio was then calculated from Eq. (6). We also utilized the following simpler equation to calculate the S_0/S_1 ratio:

$$\frac{(\varepsilon'(m) - \varepsilon'(dry))_{1\ \mathrm{MHz}}}{(\varepsilon'(m) - \varepsilon'(dry))_{0.1\ \mathrm{Hz}}} = \frac{S_0}{S_t} \tag{7}$$

Interestingly, the values of S_0/S_t calculated from Eqs. (6) and (7) (shown in Figure 15) were in excellent agreement, were in the range between 0.6 and 0.8, and did not vary systematically with exposure time. This finding parallels the result of the analysis based on the NIR data.

Of major interest in the analysis of the MIR spectra is the range between approximately 3000 and 3700 cm^{-1}, where vibrational modes due to the various forms of hydrogen bonding are located. A close-up of that spectral range in a dry sample is shown in Figure 16. Deconvolution of the spectrum of Figure 16 results in a weak absorption band at 3652 cm^{-1} and three more bands at lower frequencies. Moisture uptake has a dramatic effect on the intensity of all absorption peaks. A series of difference spectra (obtained by subtracting the spectrum of a dry sample from that of each moist sample) with exposure time at 60°C as a parameter, are shown in Figure 17. Two distinct regions are observed: 1) a relatively sharp absorption between 3600 and 3700 cm^{-1}, and 2) a broad, irregularly shaped absorption between 3600 and 3100 cm^{-1}. An example of a deconvoluted spectrum of a sample exposed to the 60°C environment is shown in Figure 18. The intensity of these absorption bands increases with exposure time, and the important question is what is the molecular origin of these changes? We first consider the narrow absorption band at higher frequency that was fit to a Gaussian function with a peak at 3639 cm^{-1}. There is little doubt that this absorption is due to the previously defined S_0 species, and that it corresponds to the 7088 cm^{-1} NIR band assigned to a combination of symmetric and asymmetric stretching of non-hydrogen bonded water. This absorption was observed in polymer networks and water-solvent mixtures, and it has been attributed to non-hydrogen-

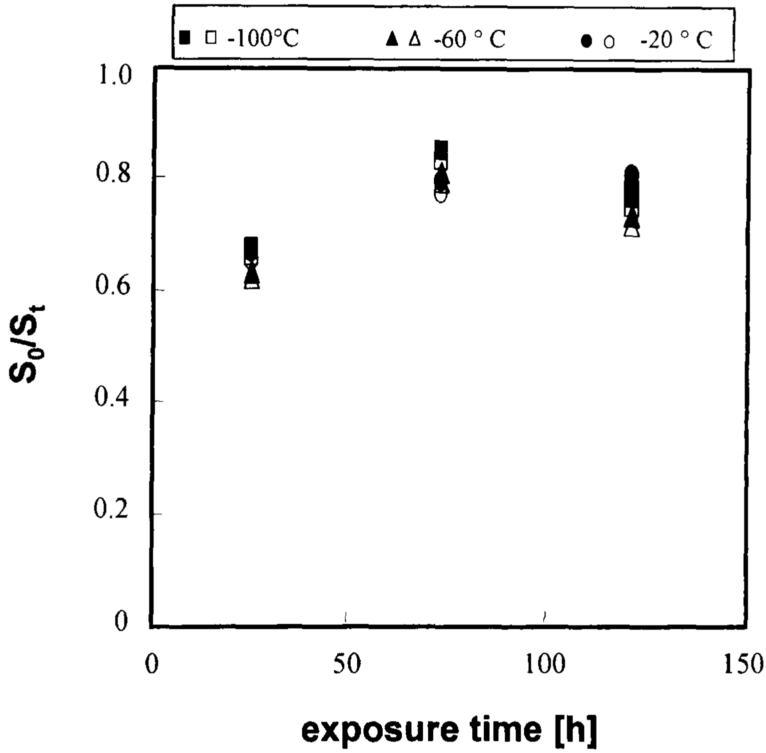

FIGURE 15 Ratio of non-hydrogen-bonded (S_0) to total (S_t) absorbed water as a function of exposure time from the DRS data: filled symbols (Eq. (7)); open symbols (Eq. (6)).

bonded water [56–58]. In our BMI network, this absorption is assigned to water molecules located in the pockets surrounded by hydrophobic moieties, such as benzene rings and or methylene bridges, where the likelihood of hydrogen bonding is low.

We next proceeded with attempts to deconvolute the broad absorption range between 3600 and 3100 cm^{-1} . The best results were obtained using three Gaussian functions, as shown in Figures 16 and 18 for dry and moist BMI networks, respectively. The absorption intensity (defined by the area under the peak) increases with increasing exposure time. The presence of several absorption bands confirms that: 1) the absorption mechanism is complex, and 2) the often-invoked but seldom justified concept of two types of absorbed moisture, commonly lumped under "loosely" and "strongly" bound water, is an oversimplification of the actual situation. But what can we

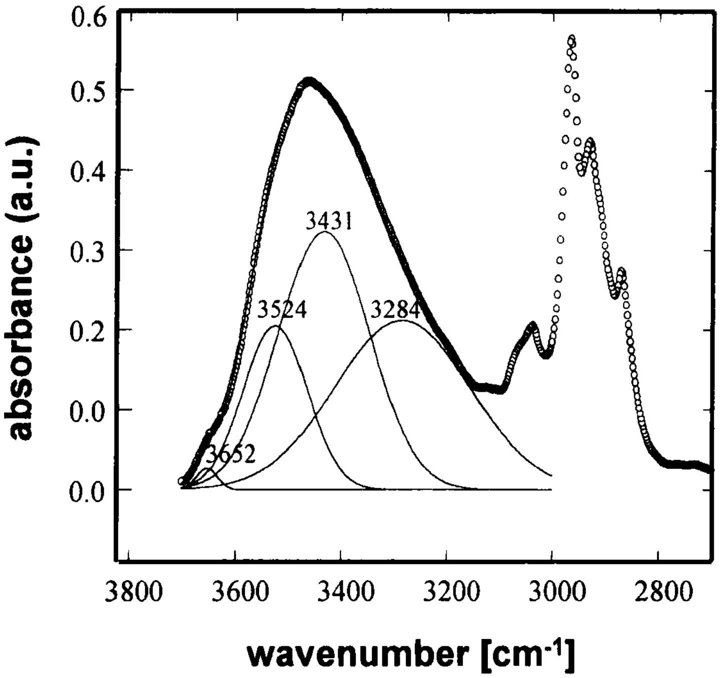

FIGURE 16 Deconvoluted MIR spectrum of cured BMI in the 3700–2800 cm^{-1} region.

say about the molecular origin of the absorption bands at 3599, 3470 and 3238 cm^{-1}? It is evident that these three bands are associated with hydrogen-bonded water, although it is not clear from the MIR spectra: 1) what specific atoms/sites on the network participate in these interactions, 2) in what order of preference (if any), and 3) how many hydrogens on a given water molecule form a hydrogen bond. In a BMI network, as argued earlier, the absorbed water could (possibly) form a hydrogen bond at several sites on the network, including the hydroxyl group, the ether oxygen, the carbonyl group, and the tertiary amine nitrogen. While the strength of hydrogen bonding interactions (and the corresponding frequency shift) is known to depend on the nature of the donor-acceptor pair, the identification of an absorption band with a particular type of hydrogen bond (*i.e.*, between water hydrogen and one of the above specified network sites) is not straightforward. The quantitative interpretation of MIR spectra is further complicated by difficulties associated with a precise measurement of the (frequency dependent) molar absorptivities for

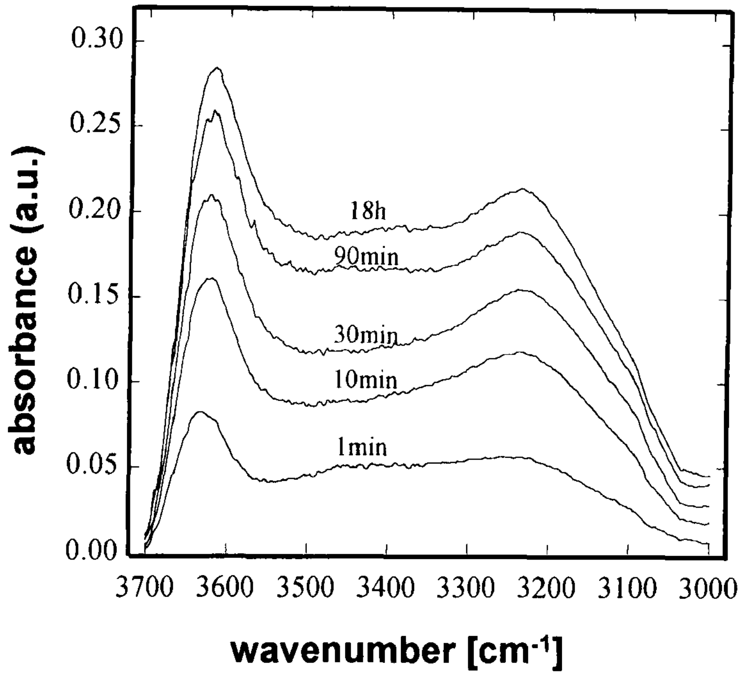

FIGURE 17 Difference spectra of cured BMI in the 3700–3000 cm^{-1} range after exposure 60°C/98% RH for different time.

various interacting pairs. Nevertheless, Musto *et al.* [39], in their study of water absorption in epoxy networks, have tentatively assigned the 3599 cm^{-1} band to the stretching mode of hydrogen-bonded water hydroxyl. However, the identity of an epoxy or BMI network site that participates in hydrogen bonding, in either S_1 or S_2 form, remains unspecified. Moreover, if the absorbed water forms dimers or trimers, there will also be a possibility of hydrogen bonding between the adjacent water molecules (S_3). It is, therefore, fair to say that, although a water molecule can participate in one (S_1) or two (S_2) hydrogen bonds, an outright quantitative identification of a MIR absorption band with a specific complex form (S_1, S_2, S_3) warrants further research. We do anticipate that the simulation study of water absorption into a BMI network, currently underway in our laboratory, will provide additional information.

A final comment regarding our efforts aimed at the development of a fundamental quantitative correlation between FTIR and DRS data is called for. This would, in effect, provide a link between the chemical

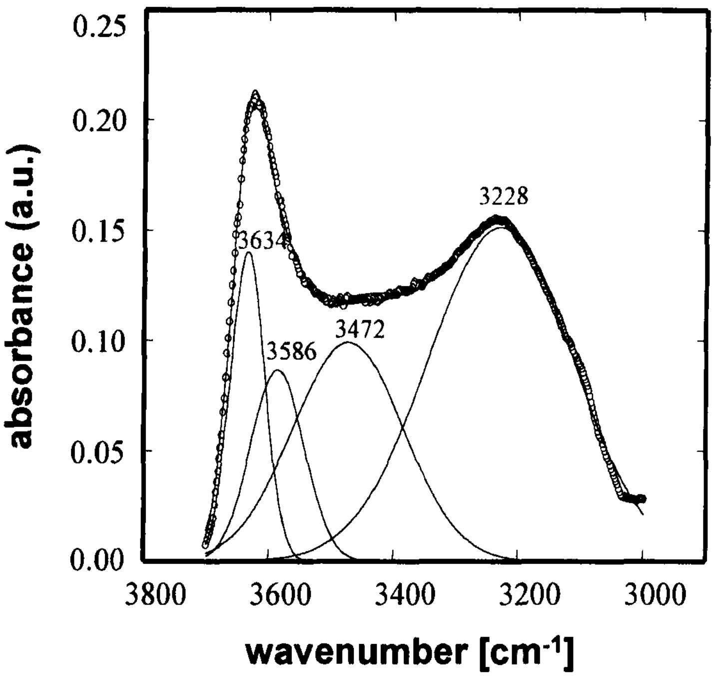

FIGURE 18 Deconvoluted MIR spectrum of cured BMI in the 3700–2800 cm^{-1} region, following exposure to 60°C/98% RH environment for 30 min.

(FTIR) and physical (DRS) phenomena that accompany water absorption into the network. Specifically, we are seeking to correlate a dielectric material parameter (such as the average relaxation time, dielectric relaxation strength, or a shape parameter(s) of the dielectric spectrum) with a fundamental parameter deduced from the FTIR spectra (*e.g.*, absorption strength, dipole type and concentration). This will be the subject of a forthcoming publication.

CONCLUSIONS

The results of this investigation provide new insight into the local molecular dynamics and the chemical interactions between bismaleimide (BMI) networks and absorbed water. Near-IR (NIR) and mid-IR (MIR) analyses revealed the presence of non-hydrogen-bonded and hydrogen-bonded water. A quantitative analysis of NIR and DRS data revealed that about 70% of the absorbed water is non-hydrogen-bonded.

The non-hydrogen-bonded water, termed S_0, is represented by the NIR and MIR absorption bands at 7088 and 3639 cm^{-1}, respectively. Characteristic absorption bands in the NIR and MIR spectra were deconvoluted, and attempts were made to match absorption bands with water molecules that participate in one (S_1) or two (S_2) hydrogen bonds. But the identification of an absorption band with a specific atom/site on the BMI network that participates in hydrogen bonding (*e.g.*, ether oxygen, hydroxyl group, carbonyl group, or tertiary amine nitrogen) was not straightforward, and additional information needs to be gained before such assignments are made.

The absorbed water molecules contribute to the development of a local relaxation process, termed γ^*. The dielectric relaxation strength of this process was observed to increase with increasing moisture uptake. Like most sub-Tg relaxations, the γ^* process is Arrhenius, with activation energy of 50 kJ/mol. The γ^* dynamics are slower than those of liquid water, the probable cause being the steric hindrance imparted by the surrounding network. One particularly important finding is that the average relaxation time for the γ^* process at temperatures above 25°C is on the order of nanosecond and, hence, its detection hinges on the ability to perform high precision dielectric measurements in the frequency range above 1 MHz. This is an important consideration in the ongoing efforts aimed at the implementation of DRS as a non-destructive inspection tool for adhesive joints.

REFERENCES

[1] A strong initiative has emerged in recent years aimed at identifying and monitoring the underlying chemistry and physics on a *molecular level*. The most recent discussion meeting on this subject was held during the Annual Review of the AFOSR Polymer Matrix Composites Program (Dr. Charles Y-C Lee, Director), Long Beach, CA, May 11–12, 2001.

[2] Gledhill, R. A. and Kinloch, A. J., *J. Adhesion* **6**, 315 (1974).

[3] Browning, C. E., *Polym. Eng. Sci.* **18**, 16 (1978).

[4] Keenan, J. D., Seferis, J. C. and Quinlivan, J. T., *J. Appl. Polym. Sci.* **24**, 2375 (1979).

[5] Rowland, S. P., Ed., *Water in Polymers* (ACS Symposium Series 127, American Chemical Society, Washington, DC, 1980).

[6] Sedlacek, B. and Kahovec, J., Eds., *Crosslinked Epoxies* (Walter de Gruyter, Berlin, 1987).

[7] Kaelble, D. H., Moacanin, J. and Gupta, A., In: *Epoxy Resins Chemistry and Technology*, May, C. A., Ed. (Marcel Dekker, New York, 1988), Chap. 6, p. 603.

[8] Apicella, A., In: *International Encyclopedia of Composites*, Lee, S. M., Ed. (VCH Publishers, New York, 1990), Vol. 2.

[9] Nairn, B. J., Dickstein, P. A., Plausinis, D. J. and Spelt, J. K., *J. Adhesion* **48**, 121 (1995).

[10] de Neve, B. and Shanahan, M. E. R., *J. Adhesion* **49**, 165 (1995).
[11] Maggana, C. and Pissis, P., *J. Polym. Sci. Part B: Polym. Phys.* **37**, 1165 (1999).
[12]
[13]
[14] Soles, C. L., Chang, F. T., Gidley, D. W. and Yee, A. F., *J. Polym. Sci. Part B: Polym. Phys.* **38**, 776 (2000).
[15] Grave, C., McEwan, I. and Pethrick, R. A., *J. Appl. Polym. Sci.* **69**, 2369 (1998).
[16] Affrossman, S., Banks, W. M., Hayward, D. and Pethrick, R. A., *Proc. Inst. Mech. Eng.* **214**, Part C, 87 (2000).
[17] Williams, G., In: *Keynote Lectures in Selected Topics of Polymer Science*, Riande, E., Ed. (CSIC, Madrid, 1997), Chap. 1, 1–40.
[18] Mijovic, J., Miura, N. and Soni, S., *J. Adhesion* **76(2)**, 123 (2001).
[19] Williams, G., "Dielectric Properties," In: *Comprehensive Polymer Science*, Allen, G. and Bevington, J. C., Eds. (Pergamon, Oxford, 1989), Vol. 2, Chap. 7, pp. 601–632.
[20] Williams, G., "Theory of Dielectric Properties," In: *Dielectric Spectroscopy of Polymeric Materials*, Runt, J. P., and Fitzegerald, J. J., Eds. (American Chemical Society, Washington, DC, 1997), Chap. 1, pp. 3–65.
[21] Williams, G., "Molecular Aspects of Multiple Dielectric Relaxation Processes in Solid Polymers", In: *Advances in Polymer Science*, Cantow, H.-J. *et al.*, Eds. (Springer-Verlag, Berlin, 1979), Vol. 33, pp. 59–92.
[22] Havriliak, S., Jr. and Negami, S., *Polymer* **8**, 161 (1967).
[23] Williams, G. and Watts, D. C., *Trans. Faraday Soc.* **66**, 80 (1970).
[24] (a) Fitz, B., Andjelic, S. and Mijovic, J., *Macromolecules* **30**, 5227 (1997); (b) Mijovic, J., Duan, Y., Miura, N. and Monetta, T., *Polymer News* **26**, 251 (2001).
[25] Kremer, F. and Arndt, M., In: *Dielectric Spectroscopy of Polymeric Materials*, Runt, J. P. and Fitzgerald, J. J., Eds. (American Chemical Society, Washington, DC, 1997), Chap. 5, p. 139.
[26] Kranbuehl, D., In: *Dielectric Spectroscopy of Polymeric Materials*, Runt, J. P. and Fitzgerald, J. J., Eds. (American Chemical Society, Washington, DC, 1997), Chap. 11, p. 303.
[27] Mijovic, J. and Andjelic, S., *Polymer* **36**, 3783 (1995).
[28] Johari, G. P. and Goldstein, M., *J. Chem. Phys.* **53**, 2372 (1970).
[29] Frisch, H. L., *Polym. Eng. Sci.* **20**, 1 (1980).
[30] Mikols, W. J., Seferis, J. C., Apicella, A. and Nicolais, L., *Polym. Comp.* **3**, 118 (1982).
[31] Apicella, A., Nicolais, L. and de Cataldis, C., *Adv. Polym. Sci.* **66**, 189 (1985).
[32] Bellucci, F. and Nicodemo, L., *Corrosion* **49**, 235 (1993).
[33] Bellucci, F., Nicodemo, L., Monetta, T., Kloppers, M. J. and Latanision, R. M., *Corrosion Sci.* **8**, 1203 (1992).
[34] Casalini, R., Corezzi, S., Fioretto, D., Livi, A. and Rolla, P. A., *Chem. Phys. Lett.* **258**, 470 (1996).
[35] Corezzi, S., Capaccioli, S., Gallone, G., Livi, A. and Rolla, P. A., *J. Phys.: Condens. Matter* **9**, 6199 (1997).
[36] Fitz, B. D. and Mijovic, J., *Macromolecules* **32**, 4134 (1999).
[37] Onsager, L., *J. Amer. Chem. Soc.* **58**, 1486 (1936).
[38] Musto, P., Mascia, L., Ragosta, G., Scarinzi, G. and Villano, P., *Polymer* **41**, 565 (2000).
[39] Musto, P., Ragosta, G. and Mascia, L., *Chem. Mater.* **12**, 1331 (2000).
[40] Barthel, J., Bachuber, K., Buchner, R. and Hetzenauer, H., *Chem. Phys. Lett.* **195**, 369 (1990).

[41] Jelinski, L. W., Dumais, J. J., Stark, R. E., Ellis, T. S. and Karasz, F. E., *Macromolecules* **18**, 1019 (1985).
[42] Jelinski, L. W., Dumais, J. J., Cholli, A. L., Ellis, T. S. and Karasz, F. E., *Macromolecules* **18**, 1091 (1985).
[43] King, J. J., Chaudhari, M. and Zahir, S., *Int. SAMPE Symp.* **29**, 394 (1984).
[44] Lee, B., Chaudhari, M. and Galvin, T., *Int. SAMPE Tech. Conf.* **17**, 172 (1985).
[45] Lind, A. C. and Fry, C. G., *ACS Proc. Div. Polym. Mater. Sci. Eng.* **59**, 466 (1988).
[46] Brown, I. M. and Sandreczki, T. C., *ACS Proc. Div. Polym. Mater. Sci. Eng.* **59**, 612 (1988).
[47] Morgan, R. J., Jurek, R. J., Yen, A. and Donnellan, T., *Polymer* **34**, 835 (1993).
[48] Mijovic, J. and Andjelic, S., *Macromolecules* **29**, 239 (1996).
[49] Rozenberg, B. A., Shin, E. E. and Morgan, R. J., *Polymer* 38, 639 (1997).
[50] Antoon, M. K., Koenig, J. L. and Serafini, T., *J. Polym. Sci. Polym. Phys. Ed.* **19**, 1567 (1981).
[51] Skrovanek, D. J., Painter, P. C. and Coleman, M. M., *Macromolecules* **19**, 699 (1986).
[52] Ngono, Y., Marechal, Y. and Mermilliod, N., *J. Phys. Chem. B* **103**, 4979 (1999).
[53] Ngono, Y. and Marechal, Y., *J. Polym. Sci. B: Polym. Phys.* **38**, 329 (2000).
[54] Three absorption bands are resolved using the Lorentzian function, yielding an excellent fit. The use of best-fit Gaussian function yields a fourth (low-intensity, high-frequency) peak, but the locations of the other three peaks are practically identical to those in the Lorentz fits.
[55] Choppin, G. R. and Violante, M. R., *J. Chem. Phys.* **56**, 5890 (1972) and references therein.
[56] Harris, D. C. and Bertolucci, M. D., *Symmetry and Spectroscopy* (Dover Publications, New York, 1989), Chap. 3, pp. 93–224.
[57] Luck, W. A. P., "Infrared Studies of Hydrogen Bonding in Pure Liquids and Solution", In: *Water, A Comprehensive Treatise*, F. Franks, Ed. (Plenum Press, New York, 1973), Vol. 2, Chap. 4.
[58] Gragson, D. E. and Richmond, G. L., *J. Phys. Chem. B* **102**, 569–576 (1998).